JCTC Journal of Chemical Theory and Computation

pubs.acs.org/JCTC Article

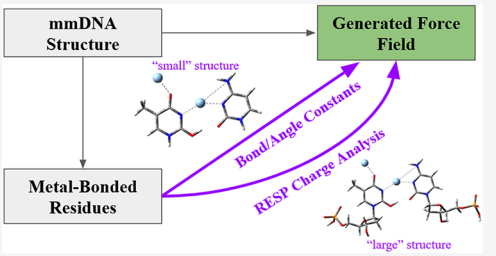
Scalable Force Fields for Metal-Mediated DNA Nanostructures

William Livernois,* Olaiyan Alolaiyan, Arpan De, and M. P. Anantram

Cite This: J. Chem. Theory Comput. 2026, 22, 2000−2012 Read Online

ACCESS | Metrics & More | Article Recommendations | Supporting Information

ABSTRACT: Force fields were developed for metal-mediated DNA (mmDNA) structures, using ab initio methods to parametrize metal coordination. Two mmDNA structures were considered, using cytosine/thymine mismatches with coordinated Ag and Hg metal atoms. These base pairs were parametrized with the proposed computational framework and subjected to multiple validation steps. The generated force fields showed enhanced structural stability within the metalated base pairs, with the coordinated metal rotating into the major groove. Our findings show a higher propeller angle associated with the metalated base pair, which agrees with previously reported experimental data. The developed force fields have the potential to unveil the structural dynamics of long metalated DNA nanowires, while results have been demonstrated on a chain of three mmDNA base pairs.



Downloaded via UNIV OF WASHINGTON on March 7, 2026 at 21:31:30 (UTC).
See https://pubs.acs.org/sharingguidelines for options on how to legitimately share published articles.

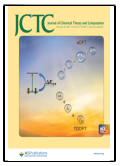
INTRODUCTION

The programmable self-assembly characteristics of DNA render it an optimal platform for fabricating nanoscale architectures with precise spatial control and structural versatility.[1] Further customizability has been demonstrated with modification of the nucleotides themselves, ranging from modification of the bases[2] to incorporation of custom functional groups.[3] Such modifications exploit the inherent Watson−Crick hydrogen bonding patterns to generate stable scaffolds. As an alternative, a transition metal can be used to mediate bonding between bases, observed between complementary bases[4] as well as between pairs of matching bases.[5−8] The incorporation of metal centers has enabled the development of DNA nanowires with higher measured conductivities than their nonmetalated counterparts.[9] The library of metal-mediated DNA or metalated DNA (mmDNA) base pairs has been expanded and extensively characterized, with recent work demonstrating that the electronic properties are highly dependent on the metal location and ligand modification.[10]

While the synthesis and characterization of mmDNA has been studied over the past 20 years, knowledge gaps remain in the structural properties of mmDNA heterostructures.[11] X-ray crystallography has been used in previous works to determine the structure of DNA bases, with resolutions ranging from 2−5 Å.[10,12,13] These methods generate 3D maps of electron density from the periodic structure, which are fitted to the known DNA base sequence to predict the structure. However, the crystal structure itself can physically constrain atom movement, leading to strained bonding across the structure. Additionally, the temperatures used for crystallization may not match the environment of a constructed nanostructure or device. To address these gaps, ab initio methods have been applied to mmDNA, with initial studies focusing on the electronic properties of metal-nucleobase interactions on single base pairs[14,15] and more recent studies extending this analysis to look at charge transport in a DNA nanostructure.[16] The dynamics of such structures have been previously studied, ranging from molecular dynamics (MD) modeling treating the coordinated metal as a lone ion[17] or directly parametrizing the metal-base bonds[18] to a hybrid quantum mechanics/molecular mechanics (QM/MM) treatment.[19,20] As the range of mmDNA base pairs continues to grow,[10,21] developing adaptable force fields for modeling complex mmDNA heterostructures has become essential, particularly for future innovations in nanodevices and biomaterials.

To address this need, we present an automated ab initio modeling approach that generates bonded terms for MD force fields, enabling efficient scaling to larger heterostructures. Rather than relying on structures generated from X-ray crystallography in a highly constrained environment, a custom force field can be constructed to allow for simulation at ambient conditions. This work builds on the method introduced by Seminario et al. to use a projection of the atomic Hessian matrix to generate force constants for bond and angle interactions.[22] To accomplish this, we have built a tool that modifies the existing *pyMSMT* software package[23] to allow parametrization of mmDNA base pairs. In this work, we have tested this tool on the recently characterized cytosine-thymine mismatch base pairs, with two metal-coordination setups: Ag atoms coordinated in two locations (referred to as C−Ag_2-T, PDB ID 7SDS) and a single coordinated Hg atom

Received: August 27, 2025
Revised: January 21, 2026
Accepted: January 22, 2026
Published: February 2, 2026



© 2026 The Authors. Published by American Chemical Society

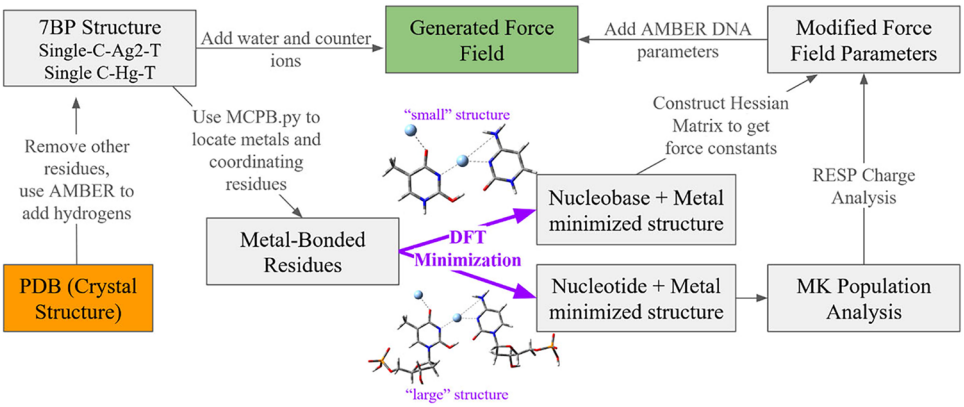


Figure 1. Flowchart for generation of force field parameters, starting with the X-ray crystallography reference structure using our patched MCPB.py. "7BP Structure" refers to the generated seven base pair structure.

(referred to as C−Hg-T, PDB ID 7SD7).[10] These were chosen due to their use of standard Watson−Crick nucleobases that are well characterized and they both contain similar metal binding sites (N3 nitrogen of Cytosine and Thymine). In addition, the C−Ag_2-T base contains metal in the major groove of the DNA, a metal modification that has not been modeled previously. For comparison, we have considered the complementary case with an A-T base pair, similarly characterized by X-ray crystallography (PDB ID 5W6W),[24] and a C-T mismatch case, without metals (referred to as the CT mismatch strand, initial structure based on PDB ID 7SDS).[10] Using the developed force fields allowed us to analyze the mmDNA electronic behavior in ambient conditions to better understand the electronic properties of constructed mmDNA nanodevices, applying the force fields to structures with more than one metal-modified DNA base pair.

METHODS

The AMBER force field used in this study parametrizes the total potential energy (E_{total}) of the system as the sum of bonded and nonbonded interactions. The total energy is expressed as

$$E_{total} = E_{bonded} + E_{non\text{-}bonded} \tag{1}$$

The bonded energy term is given by

$$E_{bonded} = \sum_{bonds} k_b(r - r_0)^2 + \sum_{angles} k_\theta(\theta - \theta_0)^2 + \sum_{dihedrals} \frac{V_n}{2}[1 + \cos(n\phi - \gamma)] \tag{2}$$

where r, θ, and ϕ are the bond length, bond angle, and dihedral angle, k_b and k_θ are the bond and angle force constants, r_0 and θ_0 are the equilibrium bond lengths and angles, and n, V_n, and γ define the dihedral parameters. The nonbonded contribution is given by

$$E_{non\text{-}bonded} = \sum_{i<j} \left[\sqrt{\epsilon_i \epsilon_j} \left(\left(\frac{R_{min,i} + R_{min,j}}{2r_{ij}} \right)^{12} - 2\left(\frac{R_{min,i} + R_{min,j}}{2r_{ij}} \right)^{6} \right) + \frac{q_i q_j}{\varepsilon r_{ij}} \right] \tag{3}$$

where distances between atoms are given by r_{ij}, Lennard-Jones (LJ) parameters are given by the van der Waals radius $R_{min,i}$ and the binding energy ϵ_i for each atom, and Coulomb interactions are modeled with atomic charges q_i and dielectric constant ε.

Equilibrium bond length and angles (r_0 and θ_0 in eq 2) were extracted from DFT minimization and force constants were derived from the generated Hessian matrix, which is given by the tensor

$$H_{i,j} = \begin{bmatrix} \frac{\partial^2 E}{\partial x_i \partial x_j} & \frac{\partial^2 E}{\partial x_i \partial y_j} & \frac{\partial^2 E}{\partial x_i \partial z_j} \\ \frac{\partial^2 E}{\partial y_i \partial x_j} & \frac{\partial^2 E}{\partial y_i \partial y_j} & \frac{\partial^2 E}{\partial y_i \partial z_j} \\ \frac{\partial^2 E}{\partial z_i \partial x_j} & \frac{\partial^2 E}{\partial z_i \partial y_j} & \frac{\partial^2 E}{\partial z_i \partial z_j} \end{bmatrix} \tag{4}$$

in Cartesian coordinates for atoms i and j. The values for k_b, k_θ, r_0 and θ_0 in eq 2 were parametrized between the coordinated metal and some DNA atoms (details discussed later). Dihedral parameters were not parametrized and set to zero for ligand−metal bonds. This was an approximation used in previous work[25] and validated in this work for mmDNA structures (see Section VII in the SI). The calculation of the RESP fitted partial charges (q_i and q_j) in eq 3 were determined using the procedure described below. The LJ parameters were assigned from previously published values fitted to the OPC water model, using parameters for the monovalent Ag^+ ion, which are $R_{min}/2$ = 1.489 Å and ϵ = 0.03566355 kcal/mol,[26] and for the divalent Hg^{2+} ion, which are $R_{min}/2$ = 1.565 Å and ϵ = 0.006311131 kcal/mol.[27] The LJ parameters were not cofitted in this work based on the implementation in MCPB.py, which was constructed under the assumption that the electrostatic interactions dominate short-range interactions for buried metal sites in proteins.[28] To explore the implications of this assumption, the relative contribution of the Coulomb and LJ parameters are analyzed for the seven base pair structures in the discussion and with accompanying figures in Section XII of the SI. In summary, our proposed parametrization is for the bonded terms of key metal-DNA interactions and leverages nonbonded terms for long-range effects to mmDNA systems.

mmDNA MCPB.py

The current version of the MCPB.py toolbox[29,30] contains force field parameters for proteins as well as the GAFF parameters for small organic molecules. Our key contribution of this work is to extend the ability of MCPB.py to determine force fields for a class of metalated DNA structures involving both native DNA bases and a modified thymine base called DTM. To achieve this, we have modified the MCPB.py toolbox to include the parmBSC1 force field[31] and have added the new residue DTM. The resulting software is called *mmDNA-MCPB.py*. While the code released has all files required to generate the force field for these two structures, the user can model other mmDNA structures that consist of the native bases and DTM. In DTM residue, the hydrogen atom originally bonded to the N3 atom is relocated to bond to the O2 atom in thymine to facilitate

https://doi.org/10.1021/acs.jctc.5c01426
J. Chem. Theory Comput. 2026, 22, 2000−2012

metal coordination (Figures S1 and S2 in Section I of SI). To validate this assumption for this base pair system, we ran additional DFT structure optimizations which demonstrate that the O2 atom is the most energetically favorable location for this hydrogen, and this has been included as section II of the SI. Note that the metal atom coordinates with both the N3 atom of DTM and the N3 atom of cytosine in the seven base pair metalated structures considered.

We consider two separate experimentally relevant seven base pair metalated DNA structures in this work. The first seven base pair structure, *Single−C-Ag*$_2$-T, contains a C−Ag$_2$-DTM base pair which has two silver atoms. The second structure, *Single−C-Hg*-T, contains a C−Hg-DTM base pair which has a single mercury atom. The other six layers of both structures are identical. See Table S1 in Section I of the SI for a list of all structures and corresponding PDB files.

We will now discuss the steps required to generate the force field for any metalated structure that involves the existing residues in parmBSC1 and DTM, and metal atoms that bond to them. The following steps are discussed in the context of the mentioned seven base pairs structures (See the flowchart in Figure 1):

(1) The experimentally obtained X-ray crystallography tensegrity triangles were the starting point.[10] The seven base pair structures were extracted from the large experimental PDB structures of the tensegrity triangle (PDB ID 7SDS and PDB ID 7SD7). Hydrogens were added to the structure using the tleap tool.

(2) From the above seven base pair structure, two substructures were excised. They are the nucleobase(C)-metal-nucleobase-(DTM) and nucleotide(C)-metal-nucleotide(DTM), referred to as *small structure* and *large structure respectively*. In the "small" structure, the two Carbon atoms connected to the sugar are terminated with Hydrogen (see Figure S1 of SI), and the net charges for DFT calculations with two Ag atoms and one Hg atoms are both set to a total of +2. For the "large" structure, the O3′ atom of the sugar on the 3′ end is capped with a hydrogen atom and the phosphorus atom on the 5′ end is capped with an OH group (see Figure S1 of SI). The net charge in the large structures with Ag and Hg were set to zero in the DFT calculations. mmDNA-MCPB.py automates the small and large structure excision and capping process, then applies the total charge to the generated Gaussian input files in the case of Ag and Hg atoms.

(3) To obtain the force constants, we perform an unconstrained DFT minimization and generate the Hessian matrix in the *small structure* (note the total charge is +2 without the phosphates). The mmDNA-MCPB.py uses the formatted checkpoint (.fchk) file from these DFT calculations. These force constants, bond lengths and bond angles go into the force field (.frcmod) file.

(4) To obtain the RESP partial charges, we first perform a DFT minimization on the *large structure* by freezing the phosphorus atoms to the coordinates specified in the input X-ray Structure. Then, the DFT partial charges are calculated using the Merz−Kollman-Besler method.[32] The log file from this calculation is sent to our mmDNA-MCPB.py, which then does the RESP fitting. In our default implementation, to obtain the RESP partial charges, the RESP fitting protocol involves the "large" structure, where the charges on 5 backbone atoms (P, OP1, OP2, O5′, O3′) and 11 sugar atoms (C5′, H5′, H5″, C4′, H4′, O4′, C3′, H3′, C2′, H2′, H2″) have the same values as in the parmBSC1 force field.[33] The RESP fitting gives us only the RESP partial charges of the nucleobase-metal-nucleobase subsystem of the "large" structure. mmDNA-MCPB.py also includes three other options for RESP fitting, which corresponds to (a) Allowing all the charges of the atoms in the ligating residues to change without restrictions, (b) Restraining the charges of the 5 phosphate backbone atoms (P, OP1, OP2, O5′, O3′) to parmBSC1 values and (c) Restraining the charges of the phosphorus atoms to parmBSC1 values.

Three mol2 files containing the RESP partial charges of each residue of the *large structure* were generated to be read by mmDNA-MCPB.py. The three mol2 files correspond to (a) DTM, (b) cytosine and (c) metal atoms (two metal atoms in the case of C−Ag$_2$-DTM and one metal atom in the case of C−Hg-DTM).

(5) mmDNA-MCPB.py will now generate a tleap input file, a force field modifier file containing the force constants (*.frcmod), and a file (*.mol2) containing the partial charges and residue information for the original seven base pair structure, which is used in the AMBER MD calculations. Note that the new bonds involving the metal atoms and DTM are specified directly in the tleap input file.

(6) We then remove any bonds involving the metal atom with a force constant (k_b) less than 5 kcal/(mol·Å^2), which makes it a nonbonded interaction both with respect to k_b and k_θ in eq 2. In addition, if $k_\theta < 0$ and $k_b > 5$ kcal/(mol·Å^2), k_b is retained while k_θ is set to 0 in eq 2. In AMBER, these changes are manually made to the tleap file. This is the "Generated Force Field" for interactions involving the metal atom in Figure 1. Their values, including the RESP charges, are given in Section III of SI. Note that mmDNA MCBP.py only generates force fields parameters for bonds and angles involving the metal atoms and the force field applied to the base/backbone C, O, N, H and P atoms remain unmodified from the parmBSC1 force field. For comparison, we also explore a force field with a larger number of parametrized bonded interactions and discuss the details in Section IV of the SI.

(7) All DFT calculations above were performed using Gaussian 16. In this paper, the B3LYP functional was used for all calculations with a mixed basis set, using the 6−31G** Pope basis set[34] for nonmetal atoms and the LANL2DZ basis set with LAN2Z effective core potentials[35] for metal atoms. A polarizable continuum model with a dielectric constant of 78, which is representative of water was used.[36] A benchmark of basis sets (specifically the all electron 3−21G basis set[37] as well as the LANL2DZ,[35] LANL2TZ,[38] and Stuttgart[39] basis sets) is given in Section V of the SI by comparing key metal−ligand equilibrium bond lengths. A benchmark of the DFT functional is also given in Section V of the SI, comparing RESP charge fitting results between the HF/6−31G* and the B3LYP/6−31G** levels of theory.

This code has been released[40] with a summary of modifications from the original MCPB.py software given in Table S4 in Section VI of the SI.

MD Simulation Setup

The AMBER 24 software package was used to run MD simulations using each of the generated force fields for the seven base pair structures. The structures were generated and solvated in a 10 Å periodic water box, adding Na^+ and Cl^- ions to neutralize the system. The MD simulations were conducted in five stages. First, the system underwent a constrained minimization, relaxing the solvent and ions while constraining the DNA and metal atoms (restraining force constant set to 50 kcal mol^{-1} Å^{-2}). Then, a second minimization stage was applied to the entire system removing restraints. Both minimizations used a nonbonded cutoff of 10.0 Å and ran for 5000 cycles each. The third heating stage raised the system's temperature from 0 to 300 K over 1 ns under constant volume (NVT) conditions, with restraints applied to the DNA and metal atom's structure. Following heating, the system was further relaxed in a fourth equilibration stage with gradually reduced restraints conducted under constant pressure (NPT). The fifth stage was a production run, conducted under constant pressure (NPT) conditions without restraints for 100 ns. As a final test of long-term stability and to confirm the initial structural observations, each structure was subjected to an additional 900 ns trajectory for a total trajectory time of 1 μs. Temperature was maintained using a Langevin thermostat and pressure was maintained using a Berendsen thermostat, both of which are implemented in the AMBER package. The

https://doi.org/10.1021/acs.jctc.5c01426
J. Chem. Theory Comput. 2026, 22, 2000−2012

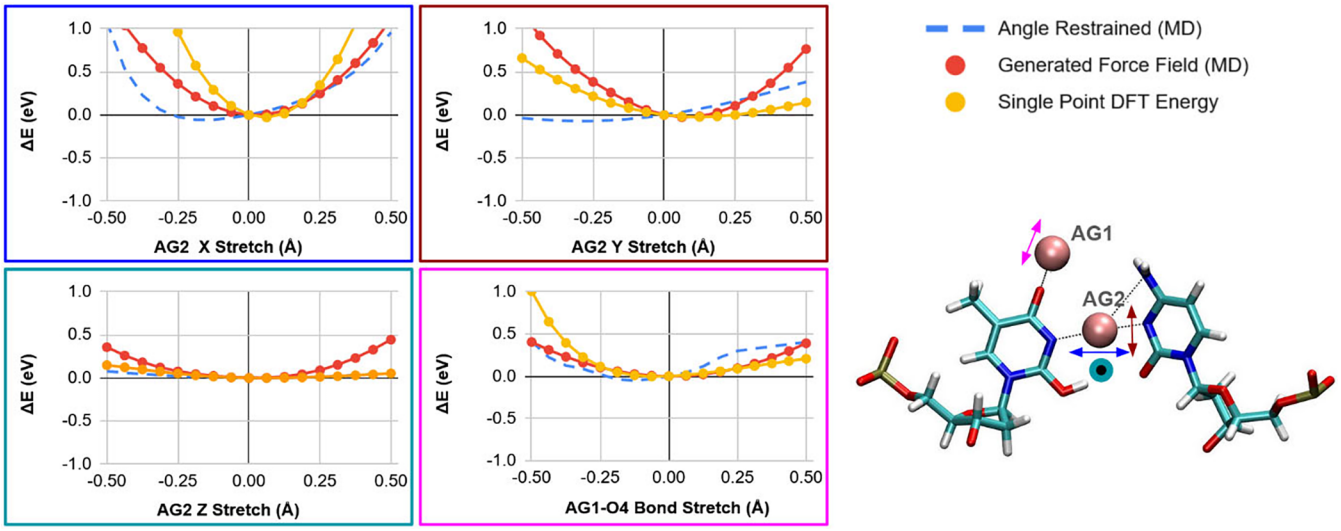


Figure 2. Comparison of energy change (ΔE) versus distance for the C−Ag_2-T large structure computed using DFT, generated force field and angle restrained force field methods. These rigid energy scans which are only for the bonds involving the metal atom are color-coded, with graphs on the left matching up with Ag atom movement given by the colored arrow on the right. AG2 refers to the coordinated Ag atom and AG1 refers to the major groove Ag atom. Only the silver atoms move in these calculations and ΔE is the deviation in energy from the MD minimized structure. The equilibrium bond lengths and bond angles are in Section III of SI.

SHAKE algorithm[41] was applied throughout to constrain bonds involving hydrogen atoms, and the Particle Mesh Ewald (PME) method[42] was used for long-range electrostatics. To analyze the structural dynamics of the DNA and metal atoms structures, we measured the RMSD using VMD[43] to observe the conformation changes during the MD simulation.

We also conducted "angle restrained force field" calculations, where the modified parmBSC1 force field[31] was used for the DNA bases while fitted nonbonding parameters were used for Ag and Hg free ions.[44,45] Instead of adding bonding parameters to parametrize the distances, harmonic restraints were applied to the N3-AG/HG-N3 bond angle (equilibrium angle set to 180°) and the O4-AG bond distances (bond distance restrained between 2.22 and 2.23 Å). The restraints were applied during and after the second stage of minimization, using a coefficient of 100 kcal/mol·radian^2 with $\theta 1$ = 170°, $\theta 2$ = 180°, $\theta 3$ = 180° and $\theta 4$ = 190°, and 100 kcal/mol·Å^2 with $R1$ = 2.02, $R2$ = 2.22, $R3$ = 2.23 and $R4$ = 2.43 Å.

RESULTS

Force fields were constructed for the seven base pair Single−C-Ag_2-T and Single−C-Hg-T sequences. To probe the effects of interactions between multiple mmDNA base pairs, a structure with three consecutive C−Ag_2-T base in a seven base pair structure was modeled with the generated force field for the Single−C-Ag_2-T structure. All structures were then subjected to energy minimization followed by 100 ns MD simulation at room temperature, analyzing structural stability and conformation changes across the simulated trajectories. The list of all structures is collected in Table S1 of the SI for clarity.

Force Field Experiments

Before developing new parametrization methods for the metal centers in the base pairs, other existing force fields were evaluated. In our initial testing, the parmBSC1 force field (modified to contain the DTM residue) was applied to the DNA atoms while nonbonded parameters for the monovalent Ag^+ free ion and divalent Hg^{2+} free ion were applied. Using these parameters, the metals were found to escape the base pairs and enter the solution, acting as counterions without any constraints on their movement. In the second iteration, the angle restrained force fields were applied to these free ions, which led to stable structures that are shown for comparison in this work. Ultimately, it was determined that the physics of these interactions was best described by multiple bonded terms and fitted onsite charges, which are parametrized with the generated force field in this work (see Table S1 in the SI for definitions of the compared cases).

To evaluate the force field fit, we first performed MD calculations on the nucleotide-AG_2-nucleotide structure using the Generated Force Field. The resulting structure was energy minimized and yielded the reference structure. The change in energy upon bond stretching was calculated relative to the reference structure (ΔE) using three different methods (Figure 2: (a) Generated Force Field, (b) DFT and (c) Angle Restrained Force Field. In these calculations of ΔE, the position of the central Ag atom was systematically displaced along the X (blue), Y (red), and Z (cyan) axes, while the major groove AG1 atom was displaced by varying the AG1−O4 distance (pink), without altering any angles in the system. The relative positions of the atoms of Cytosine and DTM were held fixed. The calculation of ΔE as a function of Ag atom displacement is referred to as *rigid energy scans*. The atomic configuration at zero displacement is the same for the three methods (x-axis of Figure 2) and corresponds to the structure obtained from the Generated Force Field.

We find that ΔE from the Generated Force Field matches closely with DFT near equilibrium, while the angle restrained force field calculation shows a larger deviation (Figure 2). The most important metal−base interaction occurs between the coordinated metal (Ag or Hg) and the N3 atoms of both cytosine and thymine in the generated force field. These interactions are characterized by symmetric bond force constants in the range of 60−85 kcal/(mol·Å^2) for Hg and 50−75 kcal/(mol·Å^2) for Ag. These values are consistent with those observed in closed-shell metal systems, such as Cu−S bonds in copper-binding enzymes (40−45 kcal/(mol·Å^2)) or Zn−N bonds in the generalized AMBER force field for zinc (30−120 kcal/(mol·Å^2)). In the C−Ag-T base pair, the major

https://doi.org/10.1021/acs.jctc.5c01426
J. Chem. Theory Comput. 2026, 22, 2000−2012

Table 1. Comparison of DFT Energies Derived from the Seven Base Pair Structures, Starting with the Original X-ray Structure and Three Structure Generation Methods Applied

System	Property	X-ray Structure	Partial DFT min	Angle Restrained	Generated Force Field
C−Ag_2-T	HOMO/LUMO gap	3.44 eV	3.48 eV	3.61 eV	3.71 eV
	HOMO energy	−5.20 eV	−5.26 eV	−5.24 eV	−5.26 eV
	relative DFT energy	0.00 eV	−20.06 eV	−25.42 eV	−25.73 eV
	RMS DFT force	12.22 eV/Å	0.64 eV/Å	0.63 eV/Å	0.62 eV/Å
C−Hg-T	HOMO/LUMO gap	3.39 eV	3.39 eV	3.61 eV	3.20 eV
	HOMO energy	−5.15 eV	−5.15 eV	−5.23 eV	−5.23 eV
	relative DFT energy	0.00 eV	−0.29 eV	−8.22 eV	−9.36 eV
	RMS DFT force	0.71 eV/Å	0.64 eV/Å	0.66 eV/Å	0.63 eV/Å

groove Ag atom (AG1) also forms a coordination bond with the thymine O4 atom, with a bond force constant (37 kcal $mol^{-1}Å^{-2}$, see Section III of SI) and a negligible angle force constant. All bonding and angle parameters are given in Section III of the SI, along with fitted charges, with more direct comparisons made to other works listed in Table 2. The parametrized metal−ligand force constants are smaller than those between organic atoms in the parmBSC1 force field, but they are sufficient to capture the stability of metal binding, thereby preserving structural integrity. As a final check of the bond and angle coefficient accuracy, we compared the values for the ligands used in the parmBSC1 force field (from parm99[46]) to the projected values from the Hessian matrix, tabulated in Table S3 of the SI. In all cases, the bonded distances are within 0.1 Å of the parm99 values, and the angles are within 3° of the parm99 values. The largest deviations are observed on the thymine residue in both cases, which tracks with noticeable interactions between the thymine oxygens and the Hg/Ag centers. Higher deviations can be seen for the projected spring constants, which are double the parm99 values for all angle spring constants in the metalated case. This may show a limitation of the fitting method used: the parm99 spring constants were fitted with a genetic algorithm that was based on experimental data. Upon availability of additional experimental data, such as absorption spectra for spring constant fitting or NMR data for structure refinement, the spring constants in this force field could be refined in addition to the metal sites. Until availability of that data, we will continue with the assumption that the refined parm99 and, by extension, the parmBSC1 parameters are the best system of values to use for this work. We have added this table as part of the benchmarking in Section V of the SI.

While torsion spring constants were not included in the generated force field, the projected values from the Hessian matrix are included as a table in Section VII of the SI. In each case, equilibrium dihedral angles for the metals are close to 0° or 180°, which would constrain the metal to the base pair plane. For the coordinated metals, this would add additional energy barriers in the *z*-direction (teal plot, in-plane direction, Figure 2) which would cause the force field to deviate farther from the ab initio result. For the case of the major groove Ag atom (AG1) the calculated spring coefficient is below those of the H3 atoms in the DTM residue. Overall, we have determined that omitting the torsion spring constants prevents additional errors from adding additional constraints to the metal centers.

Finally, we benchmark the rigid energy scans for the generated force field against the parmBSC1 force field, by displacement of the major groove Ag atom in the C−Ag_2−T base pair and the N3-bonded hydrogen in the thymine (DT) residue. As shown in Figure S6 of Section VII of SI, DFT energy profiles flatten at longer distances, in contrast to the parabolic behavior predicted by molecular mechanics, highlighting the limitations of second-order approximations at larger displacements. Moreover, this comparison also reveals limitations in DFT modeling. For example, the net charge on the displaced thymine H3 atom does not approach the expected +1, even when moved 2 Å from equilibrium, suggesting a breakdown of the mean-field approximation because a closed-shell orbital is forced to extend between components that should form an ionic pair. A similar phenomenon was observed for Ag atoms when modeled in vacuum although with the implicit water solvent model, a +1 Mulliken charge was recovered after 1 Å of displacement from equilibrium. This justifies the usage of the implicit water model that was used for all force field calculations, including for charge fitting.

DFT Energy Analysis

Applying these force fields to the seven base pair structures (Single−C-Ag_2-T and Single−C-Hg-T), the trend in DFT energies shown in Table 1 indicates that the force fields work as expected for longer DNA strands. The coordinates to calculate the DFT energies were obtained by four different methods: X-ray structure, partial DFT minimization, angle restrained force field minimization, and force field generated in this work. For both the angle restrained force field and the generated force field methods, the structure was subjected to the initial minimization, heating, and equilibration steps before a final minimization step was applied to generate the coordinates used for the DFT calculations. The partial minimization method was used in a previous work.[10] In this method, which is purely based on DFT, a force calculation was conducted to locate atoms that exceeded the specified force threshold, 5 eV/Å. Then, DFT energy minimization was applied to atoms exceeding the force threshold while keeping all other atoms of the structure frozen. The cycle was repeated until all atoms were below the 5 eV/Å force threshold cutoff. In both the Ag and Hg case, the structure determined by the generated force field gave the lowest DFT energy. It should be noted that the angle restrained force field minimization method was quite effective in both cases, reducing the DFT energy significantly, but the resulting energy scans in Figure 2 show that this method less accurately models the energy landscape around the Ag atoms.

The band gaps obtained by the four minimization methods were about ∼0.3 and ∼0.2 eV different for the Single−C-Ag_2-T and Single−C-Hg-T seven base pair structures respectively, but the LUMO orbital from our force field parametrization was quite different. In the C−Ag_2-T case, the LUMO orbital was delocalized over the major groove Ag atom with our proposed

https://doi.org/10.1021/acs.jctc.5c01426
J. Chem. Theory Comput. 2026, 22, 2000−2012

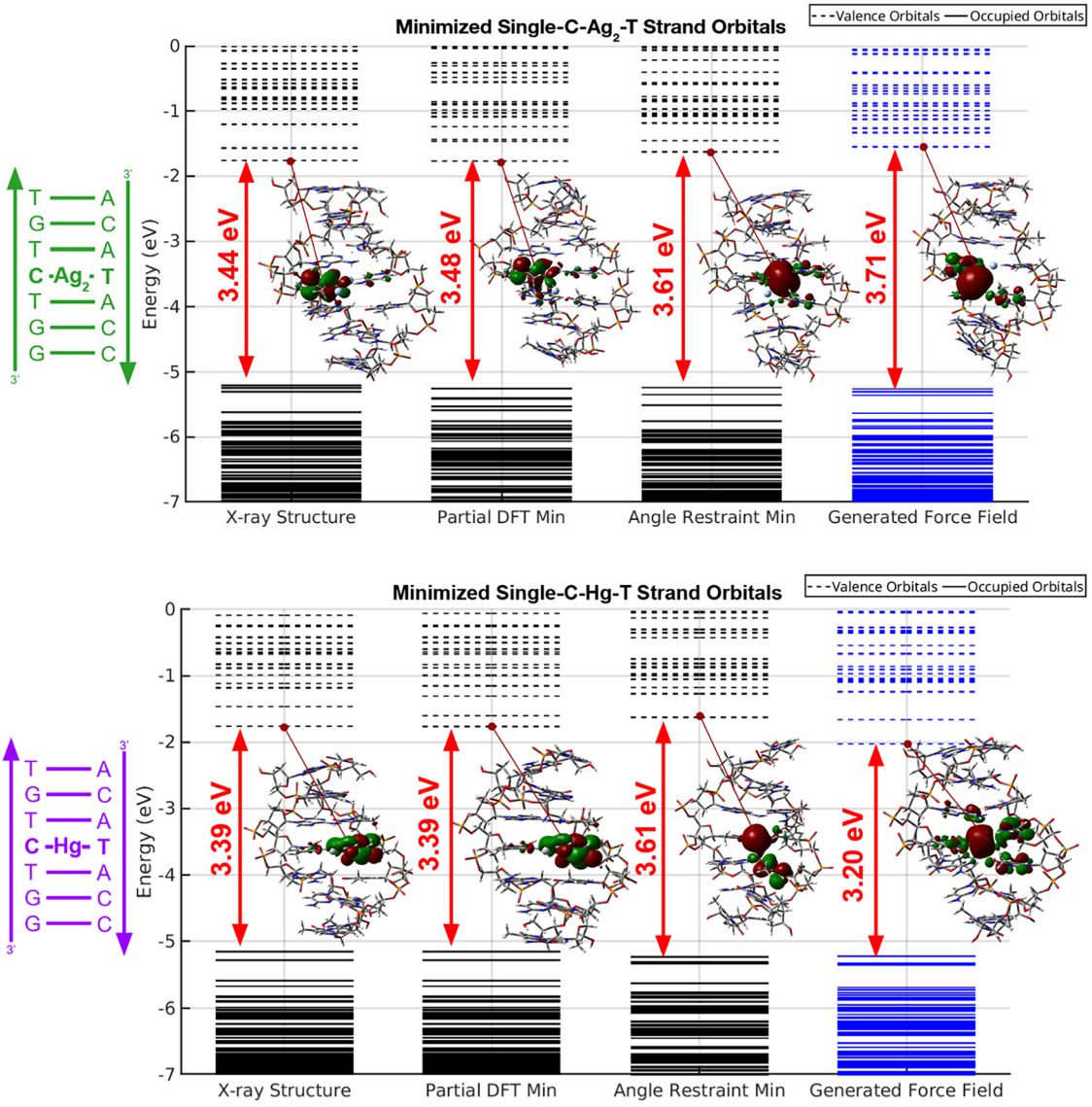


Figure 3. Side by side comparison of the seven base pair structures for the Single−C-Ag_2-T (top) and Single−C-Hg-T (bottom) seven base pair structures before and after minimization. The HOMO−LUMO gap is labeled in red for each band structure with the force field minimized case highlighted in blue. The solid and dashed lines represent the occupied and unoccupied orbitals, respectively. The coordinates have been included as PDB files in the Supporting Data.

parametrization. For the C−Hg-T case, the LUMO orbital showed more occupation of the coordinated Hg atom in addition to the surrounding base pairs. The LUMO orbitals and corresponding band structures are shown side by side in Figure 3, with our generated force field minimized case highlighted in blue.

To further obtain insight into the structure with multiple metal atoms per base pair, three parametrization methods were tested for the seven base pair Triple−C-Ag_2-T structure (see the Table in Section I of SI for the list of structures). Metal−carbon bonds were not parametrized in any of the cases. The cases are

i. Using the Generated Force Field proposed in this paper.

ii. MCPB.py used to create a force field using the Hessian matrix and DFT minimized structure for three consecutive C−Ag_2-T base pairs (see Figure S7a) with bonding cutoff set to 3.4 Å. All bonds between Ag, N, and O with k_b > 5 kcal/(mol·Å^2) are parametrized.

iii. MCPB.py used to create a force field using the Hessian matrix and DFT minimized structure for the three consecutive C−Ag_2-T structure with bonding cutoff set to 3.0 Å. All bonds between Ag, N, and O with k_b > 5 kcal/(mol·Å^2) are parametrized.

See Figure S7 in Section VIII of SI for small and large versions used to create the force field. In case (i), as a result of the 3.0 Å cutoff for bonded interactions and the 3.4 Å spacing between neighboring metal atoms, metal−metal interactions are captured solely through nonbonded LJ and Coulombic terms. For case (ii) bonded metal−metal force constants were included. In addition, for both cases (ii) and (iii), only the interactions involving metal atoms and N3 and O4 atoms on the same base pair were parametrized while retaining the parmBSC1 force field values for all other bond and angle force constants.

Applying the minimization, heating, and equilibration steps, and a final minimization step, we found that the total energy

https://doi.org/10.1021/acs.jctc.5c01426
J. Chem. Theory Comput. 2026, 22, 2000−2012

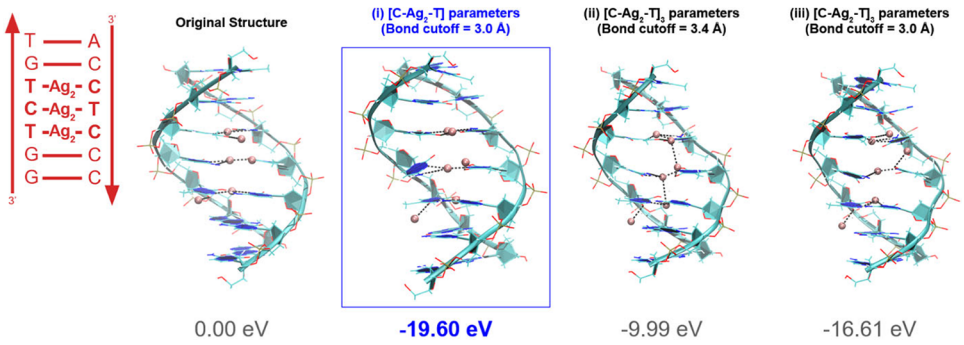


Figure 4. Constructed Triple−C-Ag_2-T base pair structure before and after minimization, comparing the three parametrization cases (i−iii), showing all new metal bonds parametrized with dotted lines. Total DFT energy relative to the original structure is labeled below each structure, The chosen force field set is case (i), labeled in blue, with the lowest DFT energy after minimization.

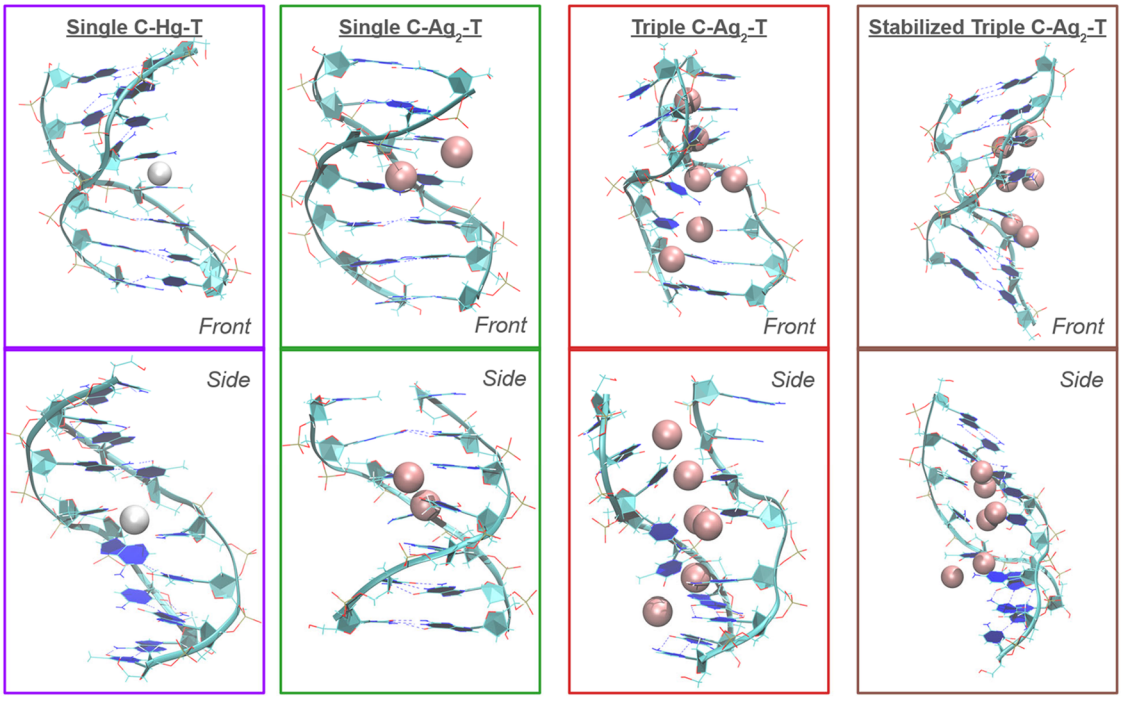


Figure 5. Final structures for each of the seven base pair metalated cases after the 100 ns trajectory and minimization using the Generated force field. A front and side view of the same structure are shown above and below in each column and labeled accordingly.

calculated using DFT dropped by the largest amount (19.6 eV) in case (i). The final structures for each of these cases are depicted in Figure 4, showing that parametrization of case (ii) created significantly more strain between neighboring base pairs. While the bonding parameters generated from case (iii) matched up closely with case (i), the N3−Ag−N3 angle changed significantly (dropping from 170 to 140°), leading to distortion of the base pair after minimization. The removal of strain in the structure in case (i) also shifted the HOMO−LUMO gap, which increased significantly after minimization (from 1.92 to 2.80 eV) and moved the LUMO orbital to the central coordinated Ag atom for case (i). Orbital energies and LUMO orbitals for each of the structures are shown in Figure S8 in the SI.

Structure Dynamics

The *Generated force field* was used to generate molecular dynamics trajectories for mmDNA structures starting with a two-step minimization run followed by equilibration run and then an initial 100 ns MD simulation. Looking at conformations during the initial trajectories, it was found that the seven base pair cases with a single metal mediated base pair, Single−C-Ag_2-T and Single−C-Hg-T, were quite stable. On the other hand, the Triple−C-Ag_2-T case was unstable with the hydrogen bonds of the capping base pair breaking apart at the AT termination, referred to as *fraying*, which is commonly seen as a precursor to DNA melting at higher temperatures.[47] This fraying occurred 10 ns into the production run, as shown in detail in Figure S10 of the SI. To stabilize this end, it was replaced with a GC base pair and is referred to as the *stabilized-Triple−C-Ag_2-T*. This structure is a symmetric sequence 3′-CCCTCCC-5′ (complementary strand 5′-GGTCTGG-3′) that remained stable throughout the 100 ns MD run. The final structures at the end of the run are shown for each of the metalated cases in Figure 5 after a final minimization step was applied. The fraying of the Triple−C-Ag_2-T is quite clear in the "front" view, with the bases pointed in opposite directions and abrupt angles observed in the backbone, while the stabilized Triple−C-Ag_2-T case stretched the structure.

https://doi.org/10.1021/acs.jctc.5c01426
J. Chem. Theory Comput. 2026, 22, 2000−2012

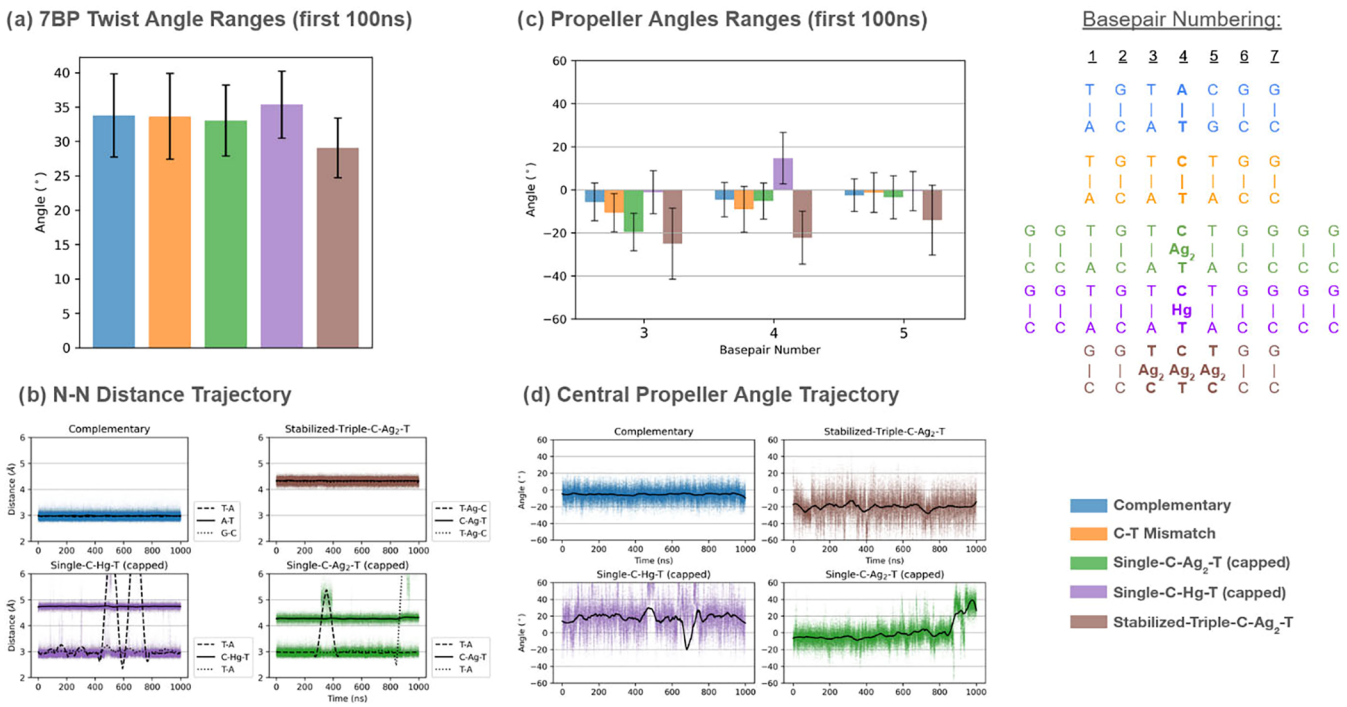


Figure 6. MD statistics using the generated force field is plotted for the five structures as applicable: (a) Twist angle ranges, averaged between the base pairs 1−7 for the first 100 ns of the trajectory, (b) spacing between coordinating nitrogen atoms for base pairs 3−5 for the complementary and metalated cases plotted along the 1 μs trajectory, (c) propeller angle ranges for base pairs 3−5 across the first 100 ns of the trajectory, and (d) central (base pair #4) propeller angles across the 1 μs trajectory for the complementary and metalated cases. These are shown for the complementary, single mismatch, capped Single−C-Ag_2-T, capped Single−C-Hg-T, and Stabilized-Triple−C-Ag_2-T cases, color coded to match the five different sequences modeled with base pair numbering given in the legend on the right. Note that the mismatch case is excluded from the 1 μs trajectory plots in (b, d) because of significant fraying. These plots are shown with an averaged value as a black line, constructed by applying a Savitzky−Golay filter across a 100 ps window with a third order polynomial to smooth the data, with the raw data shown as a scatter plot color coded to match the legend.

While a detailed discussion of the two-dimensional RMSD plots is in Section X of the SI, to understand the overall DNA structure across the trajectories, interbase pair angles and distances were calculated across the 100 ns run by saving the coordinates of 100,000 frames that were equally spaced in time. The twist angle between neighboring base pairs were calculated for the first 100 ns run and the results for the central five base pairs are shown in Figure 6a. The twist angle for all stable cases matched up closely with the values expected for B-DNA (~34°), with the exception of the stabilized-Triple−C-Ag_2-T case, which decreased to ~29° throughout the run. The base pair propeller angle was measured by taking the dihedral angle between bases in a base pair.[48] This angle averages to negative values (similar to the Complementary case) except for the seven base pair Single−C-Hg-T structure, where the propeller angle at the metalated base pair has average positive values (Figure 6c). The result of this propeller angle is shown in Figure 5, which shows the Hg atom being pushed out into the major groove in the "front" view. We see the effects of this instability when the seven base pair Single−C-Hg-T structure changes conformation briefly around 10 ns into the trajectory, shown as an inset structure to Figure S10 in the SI. Further, it showed very brief excursions to negative values (see Figure S12 of Section XI of SI). The range of each of these angles for the central three base pairs across the MD trajectory are plotted in Figure 6c. An in-depth description of the calculation methodology is presented in Section XII of the SI. As a final validation of our parametrization method, selected dihedral angles in the mmDNA base pairs (not parametrized in our force field) were analyzed over the 1 μs trajectory and are plotted in Figures S4 and S5 of the SI. Each monitored standard and improper dihedral angle were found to remain stable over the trajectory with highest fluctuations observed on the major groove AG1 atom.

Over the course of the full 1 μs MD trajectory, stability was an issue for the seven base pair strands. Both seven base pair structures extracted from crystal structures, Single−C-Ag_2-T and Single−C-Hg-T, were found to fray at the AT cap end, with final conformations shown in Figure S16 of the SI. Similarly, the nonmetalated C-T mismatch case was found to fray at the AT end, though after a longer duration (765 ns) than the metalated counterparts (403 ns for Single−C-Ag2-T and 492 ns for Single−C-Hg-T. To remove edge effects caused by the shorter seven base pair structure, double GC caps were added at both ends of the Single−C-Ag_2-T and Single−C-Hg-T strands, creating the *capped Single−C-Ag_2-T* and *capped Single−C-Hg-T* structures that were found to remain more stable for the full 1 μs duration than the corresponding non capped structures, as shown in the RMSD plots and final conformations in Figure S11 in the SI. The three metalated cases were compared to the original complementary case, which remained stable through the 1 μs run with only minor fraying of the AT base pair in position number 1 (see Figure 6). Base pair distances were analyzed across the full 1 μs trajectory, specifically monitoring nitrogen coordination of the metal in the mmDNA cases, and plotted in Figure 6b. The metal modified base pairs increased in the N−N distance by 1.4−1.6 Å compared to the complementary strand and showed

https://doi.org/10.1021/acs.jctc.5c01426
J. Chem. Theory Comput. 2026, 22, 2000−2012

Table 2. Geometry Parameter Comparisons for mmDNA Bases from Theoretical and Experimental Work, Including Parameters from This Work (Highlighted in Yellow) and Reference Parameters from the Zinc Amber Force Field (Highlighted in Pink)*

Silver (Ag) containing mmDNA Bases							
Data Type	Base Type	Charge (q)	Distance (Å)	Spring Constant (kcal mol^{-1}Å^{-1})	Propeller Angle (°)	Data Source	Ref
Theoretical studies	C-T base pair	0.45	2.23/ 2.19	51.7/ 66.6	-21.9± 10.5	MD (Prod)	*This work*
					-17.6±9.1	MD (Min)	
	C-C base pair	0.38	2.14	286.8	–	MD (wire)	51
	C-C base pair	0.38	2.14	193	-23±9	MD (wire)	18
	Zn-N3	*0.52*	*2.089*	*50.1*	–	*MD (ZAFF)*	28
Experimental Studies	C-T base pair	–	2.11/ 2.13	–	-7.4	XRC (single base pair)	10
	C/G/T duplexes	–	2.2-2.3	–	-36±8	XRC (wire)	13
	CX/TY* (wire in solution)	–	2.23/ 2.13	–	-21±4	NMR refinement	52

Mercury (Hg) containing mmDNA Bases							
Data Type	Base Type	Charge (q)	Distance (Å)	Spring Constant (kcal mol^{-1}Å^{-1})	Propeller Angle (°)	Data Source	Ref
Theoretical Studies	C-T base pair	1.30	2.45/ 2.42	85.0/ 61.2	15.3± 15.3	MD (Prod)	*This work*
					-23.1	MD (Min)	
	T-T base pair	–	2.24	–	-22	DFT (duplex)	15
	Zn-N3	*0.52*	*2.089*	*50.1*	–	*MD (ZAFF)*	28
Experimental Studies	C-T base pair	–	2.09/ 2.11	–	-29.4	XRC (single base pair)	10
	T-T base pair	–	2.0	–	-21±1	XRC (duplex)	12
	T-T base pair	–	2.0	–	-0.1±0.1	NMR refinement	53

*X and Y correspond to complementary 7-deazapurines (7-deazaguanine and 7-deazaadenosine respectively).

high stability during the MD trajectory. In the capped Single−C-Ag_2-T and capped Single−C-Hg-T cases, the nearby A-T base pairs were found to interact with the coordinated metal, which appear as peaks in the N−N distances for these neighboring base pairs. This was found to be especially true for the major groove Ag atom in the capped Single−C-Ag_2-T case, leading to a significant conformation change toward the end of the 1 μs run. Specifically, after 850 ns, the major groove Ag was found to interact strongly with the oxygen of the neighboring thymine base, which is reflected in the propeller angle plot in Figure 6d and visualized as an inset figure to the RMSD plots in Figure S11 in the SI. The effect of this interaction was also observed for the center of mass distances and backbone distances, plotted in Figure S15 in the SI. In the seven base pair Single−C-Hg-T structure, the mercury stacked in between the C and T bases along the helical axis, and this configuration remained stable. Finally, we remark that the C−Hg-T base pair showed the largest propeller angle fluctuation (Figure 6c,d), followed closely by the stabilized-Triple−C-Ag_2-T case. This is suggestive that the single point of contact between the N atoms on C and T through the coordinated metal atom causes a larger propeller angle fluctuation compared to native AT base pairs which have two Hydrogen bonds to control the propeller angle fluctuation.

In these longer trajectories, the structural results for the mmDNA bases matched those of the initial 100 ns study, including the trends in propeller angle for the metalated cases as shown in Figure 6d. In the capped Single−C-Hg-T case the propeller angle of the C−Hg-T base pair remained positive while the metalated base in the capped Single−C-Ag_2-T showed negative propeller angles across the run until the conformational change at 800 ns. The stabilized-triple−C-Ag_2-T case showed consistently negative propeller angle for each C−Ag_2-T base pair, matching up with previous observations for Ag mmDNA nanowires.[49]

DISCUSSION

Parameterization of the C-T mismatch mmDNA structures successfully created accurate force fields that can be applied to larger DNA structures. The force field parameters developed here were shown to match ab initio results with the same level of accuracy as parmBSC1 (see Figure S6 of SI). In secondary validation steps, the methodology was found to reproduce the equilibrium bond distances and angles from the parmBSC1 force field, though force constants were found to deviate from the parmBSC1 values (see Table S3 of the SI) and may require further refinement. This method of parametrization has been built as a patch to the existing MCPB.py tool and can be applied to any mmDNA base pair for use in the AMBER MD package, allowing one to look at stability of larger mmDNA heterostructures for nanotechnology applications. Scalability was specifically tested for the Ag base pair, which showed that the force field parameters developed for the single base pair was the most effective at minimizing the ab initio energy of the system. The resulting force field also demonstrated that the GC/AT cap, which contains only five hydrogen bonds, was not strong enough to cap the Triple−C-Ag_2-T structure, as shown in Figure S8. This was also found to occur during the longer 1 μs trajectories for the Single−C-Hg-T and Single−C-Ag_2-T cases, with fraying starting on the AT cap and splitting down to the central mmDNA base (frayed structures shown in Figure S16 in the SI). Adding the stronger GC/GC cap resulted in a stable structure that remained more resilient throughout the 1 μs trajectory. This shows that adding metalated base pairs to

https://doi.org/10.1021/acs.jctc.5c01426
J. Chem. Theory Comput. 2026, 22, 2000−2012

nonmetalated scaffold structures can require additional stabilization, which can inform design of mmDNA nanostructures.

The base pairs characterized in this work have never been parametrized before for MD, but our results are comparable to similar systems. Though the force constants calculated for the C−Ag_2-T base pair did not match those previously calculated for the C−Ag−C base pair, the resulting propeller angle variations matches predictions for repeating C−Ag−C nanowires.[18] The experimentally obtained propeller angles in similar (but not identical) system of stacked C−Ag−C metalated base pairs is −34°.[12,13] Detailed comparisons of key geometry parameters between this study and other works are given in Table 2. This includes a comparison to previous experimental work with structures obtained from NMR data in solution,[52,53] which shows agreement with the propeller angles observed for the Ag-modified base pairs as well as the angle ranges observed for nonmetalated base pairs during the MD trajectory.

We observe some interesting patterns across the DNA structures. In all cases, the overall width of the base pair did not change significantly between metalated and complementary base pairs. This is apparent from analysis of the distance between the C1′ atoms on the sugar during the initial 100 ns MD trajectories, which are shown in Figure S15 of the SI. In each case, the average distance remains about 10−11 Å for all bases without significant fluctuation, only increasing to slightly above 11 Å for the C-T mismatch base pair and slightly below 10 Å for the metalated base pairs. The base pairs twist into the major groove of the DNA in the metalated cases, as shown by the 1−2 Å decrease in the C1′−C1′ distance across all metalated base pairs while the base−base center of mass distance remains the same across all cases (see Figure S15 of SI). Additionally, our analysis of N−N distances in Figure 6b reveals that metal incorporation stabilizes base N−N distance fluctuations, where the triple metalated base pair structure shows markedly reduced RMSD compared to the single metal base pair, single mismatch, and fully complementary cases. Base pair propeller angles remain stable for the metalated base pairs and are higher than those of the nonmetalated cases as shown in Figure 6d. The directionality (sign) of the propeller angle was found to be different from values reported in literature for the C−Hg-T base. While our propeller angle was a small negative number after initial minimization, the average value during the MD trajectory was positive both for the 100 ns Single−C-Hg-T trajectory and the longer 1 μs capped Single−C-Hg-T trajectory. This difference is visible in the minimized 100 ns structure in Figure 5, which also showed a notable stagger distance between opposite bases in the Hg-coordinated base pair. This large structural difference can be seen directly in the fitted bond length, which is 0.2 Å higher for the Hg metal center (see purple highlighted bonds in Section III of the SI) which would lead to a combined increase of 0.4 Å spacing for that base pair. Our twist angles calculated in the Triple−C-Ag_2-T differ from those observed experimentally for similar mmDNA systems. For instance, a high-resolution crystal structure of an mmDNA Ag nanowire (PDB ID 5IX7) with one Ag atom at every base pair had an average twist angle of 36° across the strand,[49] while the average twist angle for the Stabilized-Triple−C-Ag_2-T case drops significantly across the 1 μs trajectory (Figure 6a). We attribute this to the transition from the mmDNA base, with a significant propeller angle, to the nonmetalated GC base pair caps, which is not present in prior work with continuous mmDNA nanowires,[49,50] and leads to visible distortion from the B-DNA conformation as shown in Figure 5. This also highlights the instability of the neighboring AT base pair in the Triple−C-Ag_2-T case, which leads to fraying after only a few nanoseconds, as well as in the longer trajectories of the capped Single−C-Ag_2-T and capped Single−C-Hg-T cases, where the neighboring A-T bases break apart multiple times throughout the trajectories as shown by the large N−N distance for short durations in Figure 6b. In the Single−C-Hg-T, the transition to a positive propeller angle on the C−Hg-T base pair causes the overall twist angle to increase (Figure 6a). We attribute this to the force from the larger, positively charged Hg center pushing the nearby base pairs away, which is visible in the side view in Figure 5.

While LJ parameters were not cofitted in this work, based on the previous implementation in MCPB.py and similar packages,[54] the LJ term due to the metal ion was found not to significantly impact the total MD energies. To check this assumption, we calculated the energy from the developed force field (called MD energy) for various Ag locations in the Single−C-Ag_2-T system using the four stretch directions used in Figure 2. Including effects from the seven base pair structure and screening charges with an implicit solvent, the total MD energy contribution from the LJ terms is only 3.4% compared to 46.9% from the Coulomb term (variation of about 0.01% in both cases across the trajectory). Even the contribution relative to the equilibrium energy (plotted explicitly in Figure S17 of SI) is not significant, with the LJ term only showing any visible contribution for the AG1 *z*-stretch and the AG2 bond stretch. This suggests that the approximation of using the free ion LJ parameters, rather than cofitted parameters, did not significantly impact the force fields and resulting MD trajectories for these cases. This justifies the use of the free ion parameters for this work, which can be validated upon availability of phase change data from experiment.

We have demonstrated that the generated force field can predict behavior of chemically stable mmDNA bases at ambient temperature and pressure (near 300 K and 1 bar respectively). For simulations at elevated temperatures or in conditions outside of equilibrium, such as conditions where metals may dissociate or the DNA strand melts, this force field will not accurately predict the structure. The ab initio results suggest an asymptotic energy profile as the metals dissociate from the coordinating bases (see Figure S6 in the SI), whereas the AMBER force field only fits to a second-order parabolic energy profile. Instead, fitting to a potential like the Morse potential may better predict these long-range effects, as recently implemented for the C−Ag−C base pair.[51] For applications involving switching or modulation of mmDNA base pairs, these long-range effects will be crucial for matching modeling results with experiment. Additionally, the polarization due to electric dipoles due to the metal site was not included in the parametrization. This term is a function of the valence state of the metal and has been shown to be significant for the divalent Hg state used in this study, which would require additional force field terms to model.[55] Furthermore, any effects of oxidation state or spin were not analyzed here, as the model was applied to metals with fully closed shell configurations. Spin orbit effects can impact modeling results especially with multiple metal centers. This is particularly important for heavier metals like mercury, where multiple neighboring mmDNA bases would compound to create additional spin-dependent effects. The model we have

https://doi.org/10.1021/acs.jctc.5c01426
J. Chem. Theory Comput. 2026, 22, 2000−2012

developed can serve as a starting point for such systems, with increased model complexity to be added into future work.

■ ASSOCIATED CONTENT

Data Availability Statement

Source code and associated changelogs, as well as data tables, Gaussian input files, and data analysis scripts, can be found in a publicly hosted GitHub repository: https://github.com/wliverno/pymsmt.

Supporting Information

The Supporting Information is available free of charge at https://pubs.acs.org/doi/10.1021/acs.jctc.5c01426.

Coordinates and residue information for the initial seven base pair structures along with PDB files for each of the five cases before and after MD runs (ZIP)

All supporting figures, plots, and force field data, as well as detailed descriptions of the source code and developed metrics is divided into 12 sections (PDF)

■ AUTHOR INFORMATION

Corresponding Author

William Livernois − *Department of Electrical and Computer Engineering, University of Washington, Seattle, Washington 98195, United States;* orcid.org/0000-0001-8637-1213; Email: willll@uw.edu

Authors

Olaiyan Alolaiyan − *Department of Electrical and Computer Engineering, University of Washington, Seattle, Washington 98195, United States; Center of Excellence for Green Nanotechnologies, Microelectronics and Semiconductor Institute, King Abdulaziz City for Science and Technology, Riyadh 11442, Saudi Arabia*

Arpan De − *Department of Electrical and Computer Engineering, University of Washington, Seattle, Washington 98195, United States;* orcid.org/0000-0002-2991-5293

M. P. Anantram − *Department of Electrical and Computer Engineering, University of Washington, Seattle, Washington 98195, United States*

Complete contact information is available at: https://pubs.acs.org/10.1021/acs.jctc.5c01426

Notes

The authors declare no competing financial interest.

■ ACKNOWLEDGMENTS

We are grateful to Simon Vecchioni, Ruojie Sha, and James Canary (New York University) for extensive discussion on their experimental data, which helped with the development of the force field. We would also like to thank Emre Oren (TOBB University of Economics and Technology) for the discussions. O.A. further acknowledges King Abdulaziz City for the Science and Technology fellowship. We would like to acknowledge Arman Alborzi for validation of the MD trajectory analysis. We acknowledge using the Hyak supercomputer system at the University of Washington, with student access supported by the Research Computing Club and funded by the Student Technology Fee Committee. We acknowledge NSF GCR grant number 2317843 for support.

■ REFERENCES

(1) Seeman, N. C. Nucleic Acid Junctions and Lattices. *J. Theor. Biol.* **1982**, *99* (2), 237−247.

(2) Hoshika, S.; Leal, N. A.; Kim, M.-J.; Kim, M.-S.; Karalkar, N. B.; Kim, H.-J.; Bates, A. M.; Watkins, N. E.; SantaLucia, H. A.; Meyer, A. J.; DasGupta, S.; Piccirilli, J. A.; Ellington, A. D.; SantaLucia, J.; Georgiadis, M. M.; Benner, S. A. Hachimoji DNA and RNA: A Genetic System with Eight Building Blocks. *Science* **2019**, *363* (6429), 884−887.

(3) Stulz, E. Porphyrin-Modified DNA as Construction Material in Supramolecular Chemistry and Nano-Architectonics. *Chimia* **2015**, *69* (11), 678−683.

(4) Aich, P.; Labiuk, S. L.; Tari, L. W.; Delbaere, L. J. T.; Roesler, W. J.; Falk, K. J.; Steer, R. P.; Lee, J. S. *M*-DNA: A Complex between Divalent Metal Ions and DNA Which Behaves as a Molecular Wire1. *J. Mol. Biol.* **1999**, *294* (2), 477−485.

(5) Tanaka, K.; Yamada, Y.; Shionoya, M. Formation of Silver(I)-Mediated DNA Duplex and Triplex through an Alternative Base Pair of Pyridine Nucleobases. *J. Am. Chem. Soc.* **2002**, *124* (30), 8802−8803.

(6) Miyake, Y.; Togashi, H.; Tashiro, M.; Yamaguchi, H.; Oda, S.; Kudo, M.; Tanaka, Y.; Kondo, Y.; Sawa, R.; Fujimoto, T.; Machinami, T.; Ono, A. MercuryII-Mediated Formation of Thymine−HgII−Thymine Base Pairs in DNA Duplexes. *J. Am. Chem. Soc.* **2006**, *128* (7), 2172−2173.

(7) Swasey, S. M.; Rosu, F.; Copp, S. M.; Gabelica, V.; Gwinn, E. G. Parallel Guanine Duplex and Cytosine Duplex DNA with Uninterrupted Spines of AgI-Mediated Base Pairs. *J. Phys. Chem. Lett.* **2018**, *9* (22), 6605−6610.

(8) Müller, J. Nucleic Acid Duplexes with Metal-Mediated Base Pairs and Their Structures. *Coord. Chem. Rev.* **2019**, *393*, 37−47.

(9) Toomey, E.; Xu, J.; Vecchioni, S.; Rothschild, L.; Wind, S.; Fernandes, G. E. Comparison of Canonical versus Silver(I)-Mediated Base-Pairing on Single Molecule Conductance in Polycytosine dsDNA. *J. Phys. Chem. C* **2016**, *120* (14), 7804−7809.

(10) Vecchioni, S.; Lu, B.; Livernois, W.; Ohayon, Y. P.; Yoder, J. B.; Yang, C.-F.; Woloszyn, K.; Bernfeld, W.; Anantram, M. P.; Canary, J. W.; Hendrickson, W. A.; Rothschild, L. J.; Mao, C.; Wind, S. J.; Seeman, N. C.; Sha, R. Metal-Mediated DNA Nanotechnology in 3D: Structural Library by Templated Diffraction. *Adv. Mater.* **2023**, *35* (29), No. 2210938.

(11) Clever, G. H.; Kaul, C.; Carell, T. DNA−Metal Base Pairs. *Angew. Chem., Int. Ed.* **2007**, *46* (33), 6226−6236.

(12) Kondo, J.; Yamada, T.; Hirose, C.; Okamoto, I.; Tanaka, Y.; Ono, A. Crystal Structure of Metallo DNA Duplex Containing Consecutive Watson−Crick-like T−HgII−T Base Pairs. *Angew. Chem., Int. Ed.* **2014**, *53* (9), 2385−2388.

(13) Kondo, J.; Tada, Y.; Dairaku, T.; Hattori, Y.; Saneyoshi, H.; Ono, A.; Tanaka, Y. A Metallo-DNA Nanowire with Uninterrupted One-Dimensional Silver Array. *Nat. Chem.* **2017**, *9* (10), 956−960.

(14) Brancolini, G.; Di Felice, R. Electronic Properties of Metal-Modified DNA Base Pairs. *J. Phys. Chem. B* **2008**, *112* (45), 14281−14290.

(15) Voityuk, A. A. Electronic Coupling Mediated by Stacked [Thymine-Hg-Thymine] Base Pairs. *J. Phys. Chem. B* **2006**, *110* (42), 21010−21013.

(16) Šebera, J.; Řeha, D.; Fukal, J.; Sychrovský, V. Interstrand Charge Transport within Metallo-DNA: The Effect Due to Hg(II)- and Ag(I)-Mediated Base Pairs. *J. Phys. Chem. C* **2020**, *124* (13), 7477−7486.

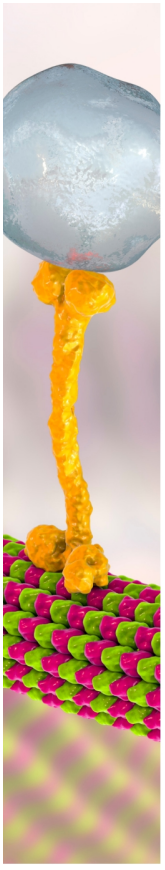
(17) Wang, Y.; Luan, B.-Q.; Yang, Z.; Zhang, X.; Ritzo, B.; Gates, K.; Gu, L.-Q. Single Molecule Investigation of Ag+ Interactions with Single Cytosine-, Methylcytosine- and Hydroxymethylcytosine-Cytosine Mismatches in a Nanopore. *Sci. Rep.* **2014**, *4* (1), No. 5883.

(18) Chen, X.; Karpenko, A.; Lopez-Acevedo, O. Silver-Mediated Double Helix: Structural Parameters for a Robust DNA Building Block. *ACS Omega* **2017**, *2* (10), 7343−7348.

(19) Bachmann, J.; Schönrath, I.; Müller, J.; Doltsinis, N. L. Dynamic Structure and Stability of DNA Duplexes Bearing a

Dinuclear Hg(II)-Mediated Base Pair. *Molecules* **2020**, *25* (21), No. 4942.
(20) Leal, L. A. E.; Karpenko, A.; Swasey, S.; Gwinn, E. G.; Rojas-Cervellera, V.; Rovira, C.; Lopez-Acevedo, O. The Role of Hydrogen Bonds in the Stabilization of Silver-Mediated Cytosine Tetramers. *J. Phys. Chem. Lett.* **2015**, *6* (20), 4061−4066.
(21) Vecchioni, S.; Ohayon, Y. P.; Hernandez, C.; Hoshika, S.; Mao, C.; Benner, S. A.; Sha, R. Six-Letter DNA Nanotechnology: Incorporation of Z-P Base Pairs into Self-Assembling 3D Crystals. *Nano Lett.* **2024**, *24* (45), 14302−14306.
(22) Seminario, J. M. Calculation of Intramolecular Force Fields from Second-Derivative Tensors. *Int. J. Quantum Chem.* **1996**, *60* (7), 1271−1277.
(23) Li, P.; Merz, K. M., Jr. MCPB.Py: A Python Based Metal Center Parameter Builder. *J. Chem. Inf. Model.* **2016**, *56* (4), 599−604.
(24) Ohayon, Y. P.; Hernandez, C.; Chandrasekaran, A. R.; Wang, X.; Abdallah, H. O.; Jong, M. A.; Mohsen, M. G.; Sha, R.; Birktoft, J. J.; Lukeman, P. S.; Chaikin, P. M.; Ginell, S. L.; Mao, C.; Seeman, N. C. Designing Higher Resolution Self-Assembled 3D DNA Crystals via Strand Terminus Modifications. *ACS Nano* **2019**, *13* (7), 7957−7965.
(25) Hoops, S. C.; Anderson, K. W.; Merz, K. M. Force Field Design for Metalloproteins. *J. Am. Chem. Soc.* **1991**, *113* (22), 8262−8270.
(26) Sengupta, A.; Li, Z.; Song, L. F.; Li, P.; Merz, K. M., Jr. Parameterization of Monovalent Ions for the OPC3, OPC, TIP3P-FB, and TIP4P-FB Water Models. *J. Chem. Inf. Model.* **2021**, *61* (2), 869−880.
(27) Li, Z.; Song, L. F.; Li, P.; Kenneth, M.; Merz, J. Systematic Parametrization of Divalent Metal Ions for the OPC3, OPC, TIP3P-FB, and TIP4P-FB Water Models. *J. Chem. Theory Comput.* **2020**, *16*, 4429−4442, DOI: 10.1021/acs.jctc.0c00194.
(28) Peters, M. B.; Yang, Y.; Wang, B.; Füsti-Molnár, L.; Weaver, M. N.; Merz, K. M., Jr. Structural Survey of Zinc-Containing Proteins and Development of the Zinc AMBER Force Field (ZAFF). *J. Chem. Theory Comput.* **2010**, *6* (9), 2935−2947.
(29) Case, D. A.; Aktulga, H. M.; Belfon, K.; Cerutti, D. S.; Cisneros, G. A.; Cruzeiro, V. W. D.; Forouzesh, N.; Giese, T. J.; Götz, A. W.; Gohlke, H.; Izadi, S.; Kasavajhala, K.; Kaymak, M. C.; King, E.; Kurtzman, T.; Lee, T.-S.; Li, P.; Liu, J.; Luchko, T.; Luo, R.; Manathunga, M.; Machado, M. R.; Nguyen, H. M.; O'Hearn, K. A.; Onufriev, A. V.; Pan, F.; Pantano, S.; Qi, R.; Rahnamoun, A.; Risheh, A.; Schott-Verdugo, S.; Shajan, A.; Swails, J.; Wang, J.; Wei, H.; Wu, X.; Wu, Y.; Zhang, S.; Zhao, S.; Zhu, Q.; Cheatham, T. E. I.; Roe, D. R.; Roitberg, A.; Simmerling, C.; York, D. M.; Nagan, M. C.; Merz, K. M., Jr. AmberTools. *J. Chem. Inf. Model.* **2023**, *63* (20), 6183−6191.
(30) Case, D. A.; Cerutti, D. S.; Cruzeiro, V. W. D.; Darden, T. A.; Duke, R. E.; Ghazimirsaeed, M.; Giambaşu, G. M.; Giese, T. J.; Götz, A. W.; Harris, J. A.; Kasavajhala, K.; Lee, T.-S.; Li, Z.; Lin, C.; Liu, J.; Miao, Y.; Salomon-Ferrrer, R.; Shen, J.; Snyder, R.; Swails, J.; Walker, R. C.; Wang, J.; Wu, X.; Zeng, J.; Cheatham, T. E., III; Roe, D. R.; Roitberg, A.; Simmerling, C.; York, D. M.; Nagan, M. C.; Merz, K. M., Jr. Recent Developments in Amber Biomolecular Simulations. *J. Chem. Inf. Model.* **2025**, *65* (15), 7835−7843.
(31) Ivani, I.; Dans, P. D.; Noy, A.; Pérez, A.; Faustino, I.; Hospital, A.; Walther, J.; Andrio, P.; Goñi, R.; Balaceanu, A.; Portella, G.; Battistini, F.; Gelpí, J. L.; González, C.; Vendruscolo, M.; Laughton, C. A.; Harris, S. A.; Case, D. A.; Orozco, M. Parmbsc1: A Refined Force Field for DNA Simulations. *Nat. Methods* **2016**, *13* (1), 55−58.
(32) Besler, B. H.; Merz, K. M., Jr.; Kollman, P. A. Atomic Charges Derived from Semiempirical Methods. *J. Comput. Chem.* **1990**, *11* (4), 431−439.
(33) Pérez, A.; Marchán, I.; Svozil, D.; Sponer, J.; Cheatham, T. E.; Laughton, C. A.; Orozco, M. Refinement of the AMBER Force Field for Nucleic Acids: Improving the Description of α/γ Conformers. *Biophys. J.* **2007**, *92* (11), 3817−3829.
(34) Petersson, G. A.; Al-Laham, M. A. A Complete Basis Set Model Chemistry. II. Open-shell Systems and the Total Energies of the First-row Atoms. *J. Chem. Phys.* **1991**, *94* (9), 6081−6090.
(35) Hay, P. J.; Wadt, W. R. Ab Initio Effective Core Potentials for Molecular Calculations. Potentials for K to Au Including the Outermost Core Orbitals. *J. Chem. Phys.* **1985**, *82* (1), 299−310.
(36) Tomasi, J.; Mennucci, B.; Cammi, R. Quantum Mechanical Continuum Solvation Models. *Chem. Rev.* **2005**, *105* (8), 2999−3094.
(37) Seeger, R.; Pople, J. A. Self-Consistent Molecular Orbital Methods. XVIII. Constraints and Stability in Hartree−Fock Theory. *J. Chem. Phys.* **1977**, *66* (7), 3045−3050.
(38) Roy, L. E.; Hay, P. J.; Martin, R. L. Revised Basis Sets for the LANL Effective Core Potentials. *J. Chem. Theory Comput.* **2008**, *4* (7), 1029−1031.
(39) Figgen, D.; Rauhut, G.; Dolg, M.; Stoll, H. Energy-Consistent Pseudopotentials for Group 11 and 12 Atoms: Adjustment to Multi-Configuration Dirac−Hartree−Fock Data. *Chem. Phys.* **2005**, *311* (1), 227−244.
(40) Livernois, W.; Li, P. Pymsmt + mmDNA, 2025. https://github.com/wliverno/pymsmt.
(41) van Gunsteren, W. F.; Berendsen, H. J. C. Algorithms for Macromolecular Dynamics and Constraint Dynamics. *Mol. Phys.* **1977**, *34* (5), 1311−1327.
(42) Joung, I. S.; Cheatham, T. E. I. Determination of Alkali and Halide Monovalent Ion Parameters for Use in Explicitly Solvated Biomolecular Simulations. *J. Phys. Chem. B* **2008**, *112* (30), 9020−9041.
(43) Humphrey, W.; Dalke, A.; Schulten, K. VMD−Visual Molecular Dynamics. *J. Mol. Graphics* **1996**, *14*, 33−38.
(44) Li, P.; Song, L. F.; Merz, K. M., Jr. Systematic Parameterization of Monovalent Ions Employing the Nonbonded Model. *J. Chem. Theory Comput.* **2015**, *11* (4), 1645−1657.
(45) Li, P.; Merz, K. M., Jr. Taking into Account the Ion-Induced Dipole Interaction in the Nonbonded Model of Ions. *J. Chem. Theory Comput.* **2014**, *10* (1), 289−297.
(46) Cheatham, T. E., III; Cieplak, P.; Kollman, P. A. A Modified Version of the Cornell et al. Force Field with Improved Sugar Pucker Phases and Helical Repeat. *J. Biomol. Struct. Dyn.* **1999**, *16* (4), 845−862.
(47) Wong, K.-Y.; Pettitt, B. M. The Pathway of Oligomeric DNA Melting Investigated by Molecular Dynamics Simulations. *Biophys. J.* **2008**, *95* (12), 5618−5626.
(48) Lu, X.-J.; Olson, W. K. 3DNA: A Software Package for the Analysis, Rebuilding and Visualization of Three-dimensional Nucleic Acid Structures. *Nucleic Acids Res.* **2003**, *31* (17), 5108−5121.
(49) Kondo, J.; Tada, Y.; Dairaku, T.; Hattori, Y.; Saneyoshi, H.; Ono, A.; Tanaka, Y. A Metallo-DNA Nanowire with Uninterrupted One-Dimensional Silver Array. *Nat. Chem.* **2017**, *9* (10), 956−960.
(50) Chen, X.; Karpenko, A.; Lopez-Acevedo, O. Silver-Mediated Double Helix: Structural Parameters for a Robust DNA Building Block. *ACS Omega* **2017**, *2* (10), 7343−7348.
(51) Gusarova, E. B.; Kovaleva, N. A. Molecular Dynamics Simulation of Melting of the DNA Duplex with Silver-Mediated Cytosine−Cytosine Base Pair. *Computation* **2024**, *12* (7), No. 145.
(52) Javornik, U.; Pérez-Romero, A.; López-Chamorro, C.; Smith, R. M.; Dobado, J. A.; Palacios, O.; Bera, M. K.; Nyman, M.; Plavec, J.; Galindo, M. A. Unveiling the Solution Structure of a DNA Duplex with Continuous Silver-Modified Watson-Crick Base Pairs. *Nat. Commun.* **2024**, *15* (1), No. 7763.
(53) Yamaguchi, H.; Šebera, J.; Kondo, J.; Oda, S.; Komuro, T.; Kawamura, T.; Dairaku, T.; Kondo, Y.; Okamoto, I.; Ono, A.; Burda, J. V.; Kojima, C.; Sychrovský, V.; Tanaka, Y. The Structure of Metallo-DNA with Consecutive Thymine−HgII−Thymine Base Pairs Explains Positive Entropy for the Metallo Base Pair Formation. *Nucleic Acids Res.* **2014**, *42* (6), 4094−4099.
(54) Abdelgawwad, A. M. A.; Francés-Monerris, A. easyPARM: Automated, Versatile, and Reliable Force Field Parameters for Metal-Containing Molecules with Unique Labeling of Coordinating Atoms. *J. Chem. Theory Comput.* **2025**, *21* (4), 1817−1830.
(55) Šponer, J.; Burda, J. V.; Leszczynski, J.; Hobzal, P. Interactions of Hydrated IIa and IIb Group Metal Cations with Thioguanine-Cytosine DNA Base Pair: Ab Initio and Density Functional Theory

Investigation of Polarization Effects, Differences Among Cations, and Flexibility of the Cation Hydration Shell. *J. Biomol. Struct. Dyn.* **1999**, *17* (1), 61−77.



CAS BIOFINDER DISCOVERY PLATFORM™

BRIDGE BIOLOGY AND CHEMISTRY FOR FASTER ANSWERS

Analyze target relationships, compound effects, and disease pathways

Explore the platform

CAS
A division of the American Chemical Society

https://doi.org/10.1021/acs.jctc.5c01426
J. Chem. Theory Comput. 2026, 22, 2000−2012